Proceedings of the Estonian Academy of Sciences
2025, **74**, 2, 222–227

https://doi.org/10.3176/proc.2025.2.25

www.eap.ee/proceedings
Estonian Academy Publishers

BIOMECHANICS

RESEARCH ARTICLE

Received 3 February 2025
Accepted 3 March 2025
Available online 16 May 2025

Keywords:
triply periodic minimal surface (TPMS), multi-surface TPMS, finite element analysis (FEA), bone tissue engineering, Johnson–Cook failure, mechanical properties, Ti6Al4V scaffolds

Corresponding author:
Mansoureh Rezapourian
mareza@taltech.ee

Citation:
Rezapourian, M. and Hussainova, I. 2025. Mechanical analysis of multi-surface TPMS lattices for bone applications. *Proceedings of the Estonian Academy of Sciences*, **74**(2), 222–227. https://doi.org/10.3176/proc.2025.2.25

Mechanical analysis of multi-surface TPMS lattices for bone applications

Mansoureh Rezapourian and Irina Hussainova

Department of Mechanical and Industrial Engineering, Tallinn University of Technology, Ehitajate tee 5, 19180 Tallinn, Estonia

ABSTRACT

Triply periodic minimal surfaces (TPMSs) offer customizable geometric and mechanical properties, making them highly suitable for bone tissue engineering. This study numerically analyzed five multi-surface TPMS lattice designs – PDL, PNG, PLG, SDL, and DNG – combined from six types of TPMSs: P (Primitive), D (Diamond), L (Lidinoid), G (Gyroid), S (Split-P), and N (Neovius), considering Ti6Al4V as the material. Geometric features, such as surface area (*SA*) and surface area-to-volume ratio (*SA/VR*), as well as mechanical properties, including elastic modulus (*E*), yield stress (*Y*), maximum compressive strength (*CM*), and energy absorption (*EA*), were evaluated through a quasi-static compression test. The multi-surface lattices exhibited smoother failure patterns, higher *EA*, and enhanced geometric features, including higher *SA/VR* compared to single lattices. PLG achieved the highest *EA*, while SDL demonstrated superior *CM* and the highest *SA* and *SA/VR*, highlighting its superior geometric complexity. Single lattices, such as D and S, exhibited higher *E* but showed brittle failure. These results underscore the potential of combining TPMSs for optimized scaffold designs in biomedical engineering.

1. Introduction

Bone tissue engineering addresses the limitations of conventional bone replacement methods, such as autografts and allografts, by utilizing engineered scaffolds that mimic the hierarchical structure of natural bone (Liu et al. 2024). These scaffolds require precise control over porosity, mechanical properties, and biocompatibility to ensure successful integration with native tissue (Musthafa et al. 2023; Liu et al. 2024). Triply periodic minimal surfaces (TPMSs) have emerged as promising scaffold designs due to their unique geometrical properties, such as high surface area-to-volume ratios and interconnected porosity (Rezapourian et al. 2022; Rezapourian et al. 2023), which facilitate nutrient transport, vascularization, and mechanical stability (Lu, Y. et al. 2022; Lv et al. 2022; Rasheed et al. 2023). Recent advancements in computational design have enabled the development of tailored TPMS architectures, offering enhanced control over mechanical and biological properties (Yin et al. 2021; Verma et al. 2022; Rezapourian et al. 2024; Vigil et al. 2024).

Titanium alloys, particularly Ti6Al4V, are widely recognized as ideal materials for bone scaffolds due to their biocompatibility, corrosion resistance, and mechanical strength (Wang et al. 2023; Zhang et al. 2023). The elastic modulus of Ti6Al4V closely matches that of natural bone, minimizing stress shielding and ensuring effective load transfer during physiological activities (Su et al. 2022; Zhang et al. 2023). Additive manufacturing techniques, such as selective laser melting (SLM), allow for the precise fabrication of complex TPMS-based scaffolds from Ti6Al4V, ensuring high fidelity and reproducibility (Zhu et al. 2022; Jiang et al. 2024). Furthermore, the fatigue resistance of the material and its ability to endure cyclic loading make it highly suitable for long-term orthopedic applications (Lei et al. 2022; Wang et al. 2023).

Finite element analysis (FEA) plays a critical role in evaluating the mechanical reliability and failure mechanisms of TPMS-based scaffolds under quasi-static loads (Rezapourian et al. 2021; Lei et al. 2022; Lu, Y. et al. 2022; Rezapourian and Hussainova 2023). By simulating stress distribution, deformation patterns, and potential failure mechanisms, FEA enables a comprehensive assessment of scaffold performance (Jin et al. 2022; Lu, S. et al. 2022). This study utilizes FEA to investigate the mechanical behavior of multi-surface TPMS architectures fabricated from Ti6Al4V under quasi-static compression loads, offering valuable insights into their potential applications in bone tissue engineering (Zhu et al. 2022; Yang et al. 2024).

2. Materials and methods

The multi-surface TPMS lattice structures analyzed in this study were designed using five unique combinations of different TPMS lattices, including P (Primitive), D (Diamond), L (Lidinoid), G (Gyroid), S (Split-P), and N (Neovius), as follows: PDL (Primitive-Diamond-Lidinoid), PNG (Primitive-Neovius-Gyroid), PLG (Primitive-Lidinoid-Gyroid), SDL (Split-P-Diamond-Lidinoid), and DNG (Diamond-Neovius-Gyroid). Figure 1 shows the generated multi-surface lattices. The base geometries for these combinations were selected to explore diverse architectural configurations. Each lattice structure was enclosed within a cubic volume measuring 20 × 20 × 20 mm in the *X*, *Y* and *Z* directions, with a unit cell size of 4 × 4 × 4 mm in each direction.

To generate the designs, remapped fields of the individual TPMS surfaces were initially created. These fields were then combined to form the multi-surface TPMS structures. The thickness of the final multi-surface lattices was determined based on a target relative density (*RD*) of 30%. The thickness of each lattice was adjusted to achieve this *RD*, resulting in the following thickness values: PDL: 0.123, PNG: 0.103, PLG: 0.135, SDL: 0.147, DNG: 0.138 mm.

The designs were created using nTop software (version 5.11.2), which also facilitated the calculation of key geometric features, such as surface area (*SA*) and surface area-to-volume ratio (*SA*/*VR*), through built-in analysis blocks. The field-driven design tool was employed to generate mapping fields for individual TPMS surfaces, while Boolean operations and thicken surface modules were used to combine TPMS surfaces and define shell thickness. Additionally, surface area analysis and volume analysis functions within nTop blocks were used to compute *SA* and *SA*/*VR*, ensuring accuracy and reproducibility in geometric feature assessment.

This systematic approach ensured that each lattice design met the desired structural and geometric criteria, enabling a robust foundation for subsequent mechanical analysis. The selected lattice combinations were chosen to explore the interaction of distinct TPMS architectures, leveraging their unique geometric and mechanical properties. These combinations were strategically selected based on their potential to optimize structural and mechanical performance for diverse applications. They provide a broad range of architectural properties, enabling meaningful insights into their mechanical behavior under quasi-static loads. By leveraging the complementary attributes of individual TPMS surfaces, these designs aim to achieve enhanced performance in bone tissue engineering and other advanced applications.

3. Finite element analysis

Once the geometry was finalized, a linear tetrahedral mesh with an element size of 0.5 mm was applied to the lattice structures in nTop software. The resulting mesh files were then exported in *.inp* format and imported into ABAQUS for FEA. Each lattice structure was positioned between two rigid plates: the bottom plate was fixed in all directions, while the top plate was constrained in all directions except along the loading direction (*Z*-axis). A displacement of 20 mm was applied to the top plate over 2 seconds, resulting in a displacement speed of 1000 mm/s. This displacement speed controlled the movement of the plate and was used to evaluate the mechanical response of the TPMS structures. The force evolution over time was extracted from the simulation results to assess the actual loading rate. The elastic-plastic material model and the Johnson–Cook failure model were adopted for the simulations, with material parameters obtained from a previous

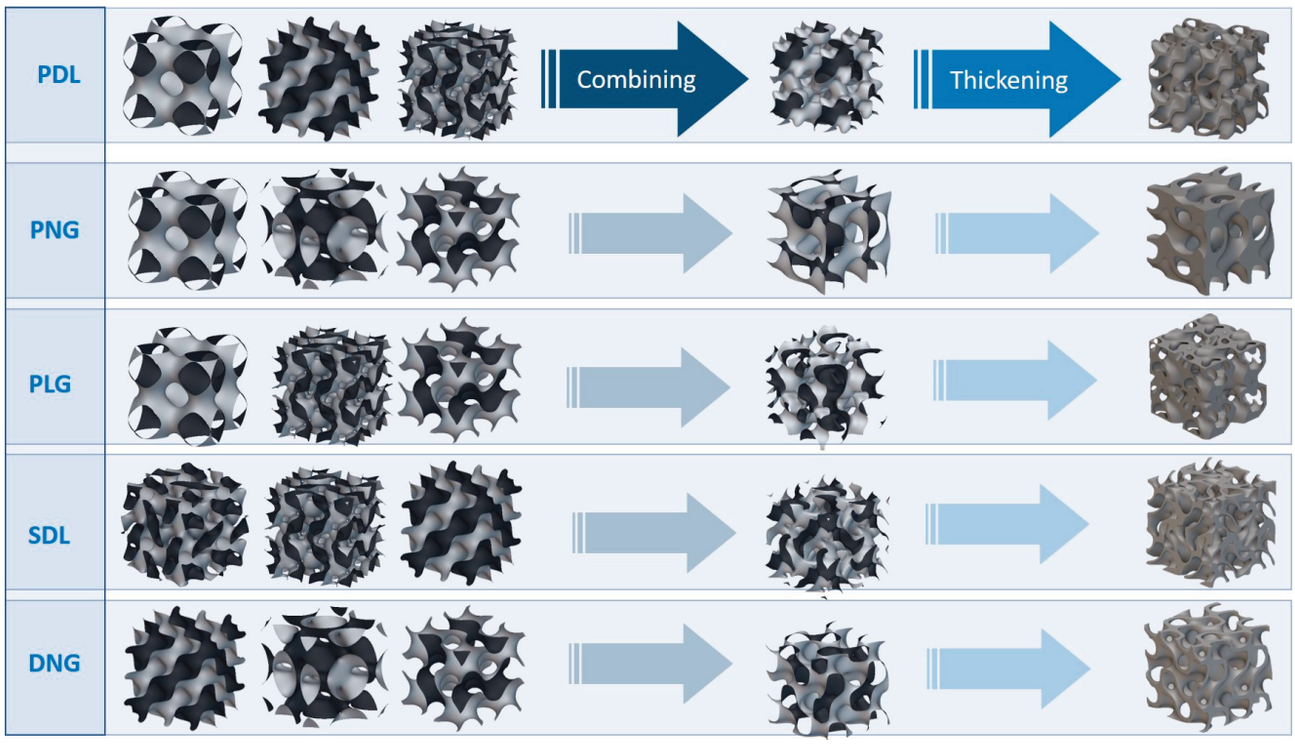

Fig. 1. Multi-surface TPMS lattices designed in this study: surface-based and thickened structures.

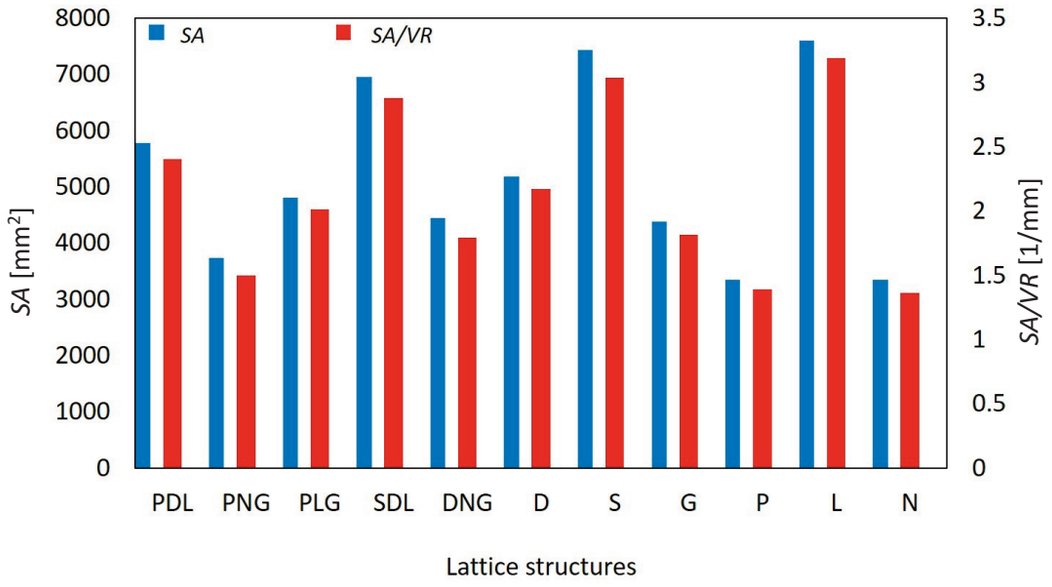

Fig. 2. Geometric features (*SA* and *SA*/*VR*) analysis of single TPMS lattices and multi-surface lattice combinations.

study (Wang and Li 2018). This simulation setup enabled a detailed analysis of the failure behavior and mechanical response of the multi-surface TPMS lattices under quasi-static loading conditions.

4. Results and discussion

4.1. Geometric features analysis

The analysis of *SA* and *SA*/*VR* revealed significant differences among the individual lattice structures and their combinations. Among the individual lattices, L demonstrated the highest *SA* and *SA*/*VR*, making it the most effective for applications requiring maximum surface exposure and porosity, such as tissue engineering and fluid flow. S followed closely, with high *SA* and *SA*/*VR*, indicating its suitability for similar applications where surface contact is critical. D, with moderate *SA* and *SA*/*VR*, offers a balance between *SA* and structural integrity, making it versatile for load-bearing applications. In contrast, P and N showed significantly lower performance, limiting their suitability for high-performance applications.

For multi-surface lattice combinations, SDL emerged as one of the best-performing configurations. The combination of S, D, and L provides a balance of high *SA* and moderate *SA*/*VR*, making it suitable for applications where both porosity and structural robustness are required. Similarly, PLG demonstrated moderate performance, combining the geometrical features of P, L, and G, though its *SA* and *SA*/*VR* values are lower compared to SDL, which might limit its effectiveness in demanding applications. PDL offers a reasonable combination of *SA* and porosity, making it a viable option for general applications, though it falls behind SDL and L in terms of performance. DNG and PNG ranked lower in both metrics, with PNG being the least effective combination due to its limited *SA* and porosity.

In conclusion, L is the most effective individual lattice for maximizing *SA* and porosity, followed by S and D. Among the combinations, SDL emerges as the best-performing configuration, followed by PDL and PLG, while DNG and PNG are the least favorable. These rankings highlight the importance of selecting appropriate lattice structures or combinations based on the specific requirements for bone applications. Figure 2 compares geometric features of single TPMS and multi-surface lattices.

4.2. Comparative analysis of lattice structures: failure mechanism and mechanical properties

The mechanical behavior of the multi-surface and single TPMS lattices was analyzed under a compression test. Their performance was evaluated based on elastic modulus (*E*), yield stress (*Y*), maximum compression strength (*CM*), and energy absorption (*EA*), providing insights into failure mechanisms, plateau stress regions, and breakage patterns. Table 1 presents the mechanical properties of multi-surface and single TPMS lattices.

According to Fig. 3, the SDL lattice demonstrates superior load distribution and a more gradual failure mechanism, while the PLG lattice, though capable of higher energy absorption, exhibits localized failure at stress-concentrated regions. These

Table 1. Mechanical properties of multi-surface and single TPMS lattices under a compression test

	PDL	PNG	PLG	DNG	SDL	P	D	L	N	G	S
E [MPa]	7954.22	9914.32	9078.16	5069.60	10 728.29	8887.65	13 733.96	4561.84	5802.42	10 684.93	14 106.80
Y [MPa]	126.19	133.13	133.86	98.85	126.32	92.65	109.05	198.10	175.46	136.81	141.90
CM [MPa]	161.13	224.55	201.89	192.26	253.45	182.29	257.76	290.12	230.37	247.65	316.24
EA [J]	266.79	261.78	291.19	218.23	286.71	267.45	271.61	208.96	263.16	271.54	269.13

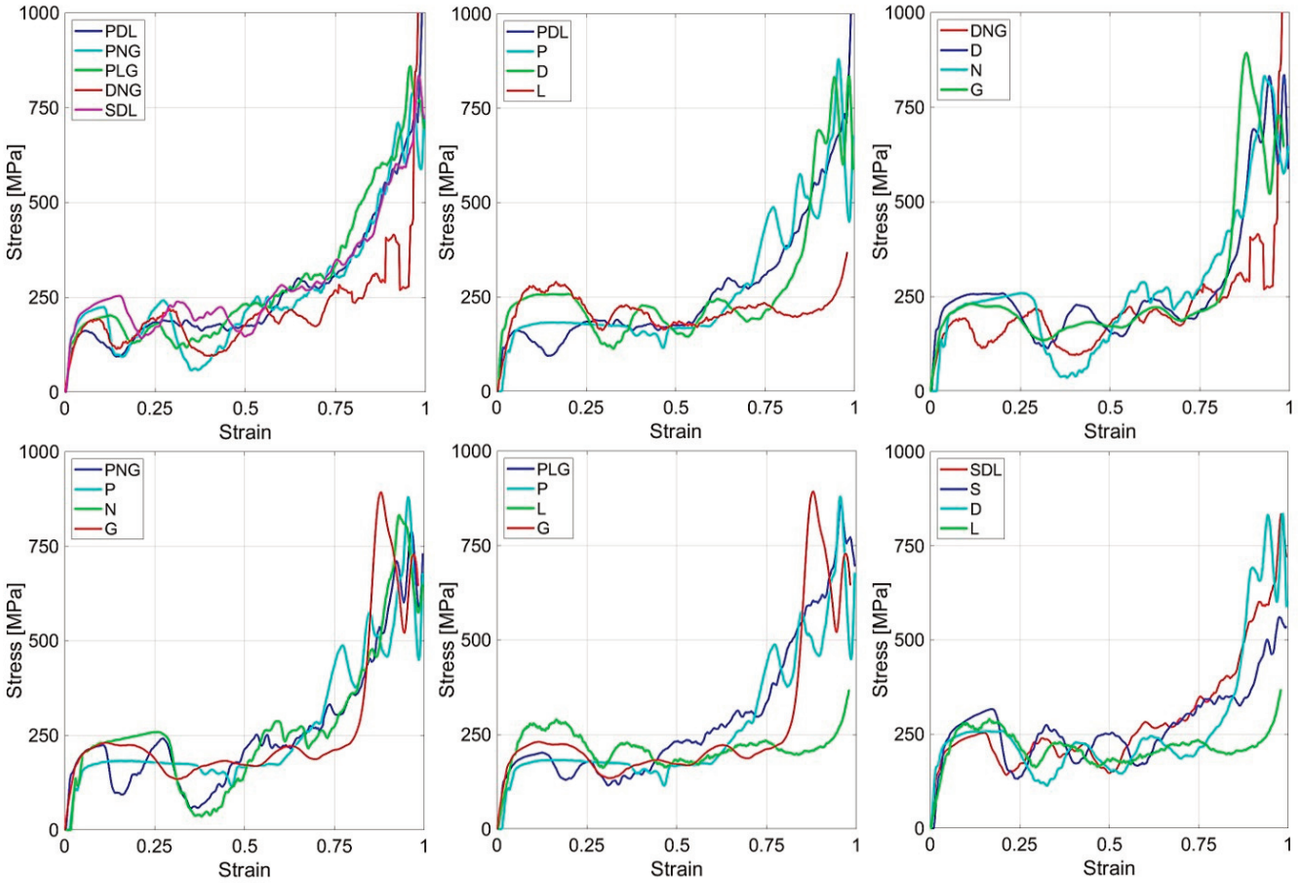

Fig. 3. Stress-strain curve of single TPMS lattices and multi-surface lattice combinations.

differences underscore the impact of lattice geometry on stress and strain distribution, as well as the mechanical stability of the structures under compression.

- PDL vs. P, D, and L: PDL exhibited lower *E* and *CM* compared to P and D, but demonstrated smoother failure and greater plateau stress than L, showcasing intermediate properties.
- PNG vs. P, N, and G: PNG outperformed P and G in *CM*, with comparable *EA* to N, and smoother failure than P and N.
- PLG vs. P, L, and G: PLG surpassed L and G in *E* and *EA*, with a prolonged plateau region, offering the highest *EA* among all configurations.
- DNG vs. D, N, and G: DNG demonstrated lower *E* but showed balanced strength and ductility. It exhibited early failure but remained suited for lightweight designs.
- SDL vs. S, D, and L: SDL achieved comparable *CM* to S and D, with superior *EA* and smoother failure behavior, making it ideal for gradual load-bearing applications.

Multi-surface lattices, such as PLG and SDL, exhibited smoother failure patterns and extended plateau regions, dissipating more energy before collapse. Single lattices, especially D and S, showed higher strength but displayed brittle failure behavior. The pronounced plateau regions in SDL, D, and S supported sustained loading without abrupt collapse.

In summary, multi-surface lattices such as PLG and SDL offer balanced strength, energy absorption, and gradual failure, while single lattices such as D and S excel in strength but show brittleness. These results highlight the potential of combining lattice architectures for optimized performance.

The von Mises stress (S) and plastic strain (PEEQ) distributions for the SDL and PLG lattices under 25%, 50%, and 75% strain (corresponding to 5, 10, and 15 mm compression), as shown in Fig. 4, reveal key deformation and failure mechanisms. At 25% strain, stress concentrates at the unit cell connections, particularly in thinner regions, marking the onset of deformation. Plastic strain is minimal and localized to these areas. At 50% strain, stress spreads across the layers and connections, with significant plastic strain indicating progressive weakening. By 75% strain, stress peaks lead to critical failures, with plastic deformation concentrated at key junctions. The SDL lattice shows a more uniform failure progression, while the PLG lattice undergoes abrupt, localized collapses in stress-concentrated regions. These differences highlight the impact of geometry on stress distribution and structural stability under compression.

The PDL lattice exhibited moderate properties in terms of *E* and *Y* but showed the lowest *CM* and *EA*. In contrast, PNG demonstrated higher *E* and *CM* but lower *EA*. The PLG lattice showed balanced performance, achieving the highest *EA* and exhibiting gradual failure after *CM*. The DNG lattice had the lowest *E*, moderate *CM*, and limited energy absorption. SDL outperformed the other multi-surface lattices, with high *CM* and significant *EA*.

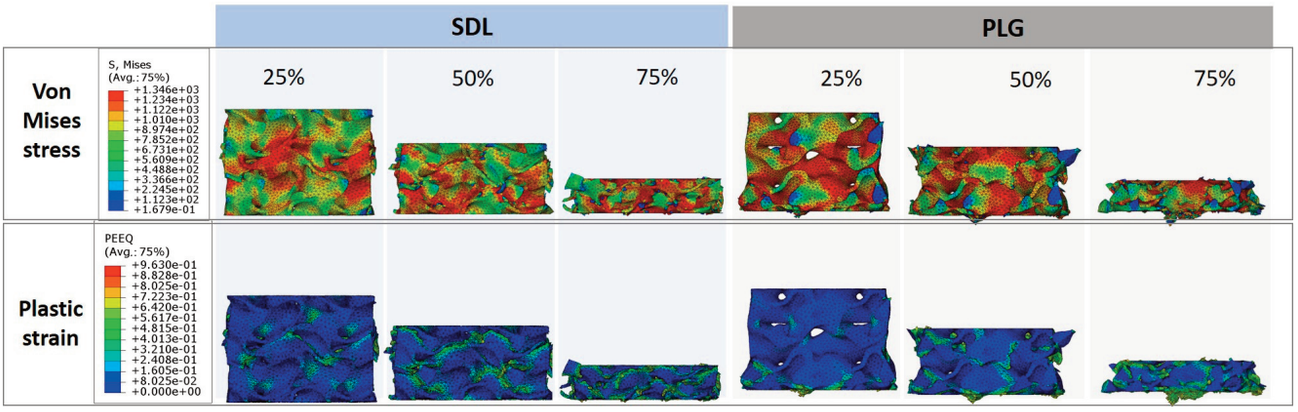

Fig. 4. Von Mises stress distribution and plastic strain for SDL and PLG multi-surface lattice samples.

5. Conclusions

This study evaluated the geometric and mechanical properties of multi-surface TPMS lattices and single lattices under a compression test. The findings highlight significant differences in performance, with multi-surface lattices offering a balance between strength, energy absorption, and failure behavior, while single lattices excelled in load-bearing capacity but exhibited brittle failure. The results underscore the potential of combining lattice architectures to achieve optimized mechanical properties tailored to specific applications.

- Geometric features: Multi-surface lattices such as PLG and SDL exhibit higher *SA/VR* values, enhancing energy absorption and load distribution. Single lattices such as D and S achieve high surface areas, contributing to their superior strength.
- Mechanical properties: Multi-surface lattices provide a balance of mechanical performance, with SDL and PLG excelling in energy absorption and smooth failure behavior. Single lattices such as D and S demonstrate higher elastic moduli and maximum compression strengths but exhibit brittle failure. PLG achieved the highest energy absorption among all lattices, making it ideal for applications requiring resilience and gradual failure. SDL combined high strength and a well-defined plateau region, making it suitable for load-bearing applications with sustained energy dissipation.
- Failure behavior: Multi-surface lattices generally showed smoother failure patterns and extended plateau regions, enhancing energy dissipation and stability. Single lattices exhibited sharper failures post-maximum compression strength, indicating brittleness but higher load-bearing capacity. These findings emphasize the potential of multi-surface lattices for applications requiring balanced mechanical properties and smooth failure behavior, while single lattices remain suitable for strength-critical tasks.

Data availability statement

All data are available in the article.

Acknowledgments

This work was supported by the Estonian Research Council under grant PRG643 (Irina Hussainova), and the M-ERA.Net project “BiLaTex” MNHA23020. The publication costs of this article were partially covered by the Estonian Academy of Sciences.

References

Jiang, J., Huo, Y., Peng, X., Wu, C., Zhu, H. and Lyu, Y. 2024. Design of novel triply periodic minimal surface (TPMS) bone scaffold with multi-functional pores: lower stress shielding and higher mass transport capacity. *Front. Bioeng. Biotechnol.*, **12**, 1401899.

Jin, S., Yamamoto, Y., Harada, Y., Kaneko, S., Oishi, K. and Ishibashi, Y. 2022. Effectiveness of photofunctionalized titanium alloy on osseointegration in rats with type 2 diabetes. *J. Orthop. Surg. Res.*, **17**(1), 445.

Lei, P., Qian, H., Zhang, T., Lei, T., Hu, Y., Chen, C. et al. 2022. Porous tantalum structure integrated on Ti6Al4V base by Laser Powder Bed Fusion for enhanced bony-ingrowth implants: in vitro and in vivo validation. *Bioact. Mater.*, **7**, 3–13.

Liu, Z., Dong, W., Shi, Z., Pei, J., Ma, T. and Fu, K. 2024. Mechanistic study on the role of 3D-printed biomimetic coral bone scaffolds in bone defect repair. *Appl. Comput. Eng.*, **63**, 62–67.

Lu, S., Jiang, D., Liu, S., Liang, H., Lu, J., Xu, H. et al. 2022. Effect of different structures fabricated by additive manufacturing on bone ingrowth. *J. Biomater. Appl.*, **36**(10), 1863–1872.

Lu, Y., Huo, Y., Zou, J., Li, Y., Yang, Z., Zhu, H. et al. 2022. Comparison of the design maps of TPMS based bone scaffolds using a computational modeling framework simultaneously considering various conditions. *Proc. Inst. Mech. Eng. H*, **236**(8), 1157–1168.

Lv, J., Jin, W., Liu, W., Qin, X., Feng, Y., Bai, J. et al. 2022. Selective laser melting fabrication of porous Ti6Al4V scaffolds with triply periodic minimal surface architectures: structural features, cytocompatibility, and osteogenesis. *Front. Bioeng. Biotechnol.*, **10**, 899531.

Musthafa, H.-S. N., Walker, J., Rahman, T., Bjørkum, A., Mustafa, K. and Velauthapillai, D. 2023. In-silico prediction of mechanical behaviour of uniform gyroid scaffolds affected by its design parameters for bone tissue engineering applications. *Computation*, **11**(9), 181.

Rasheed, S., Lughmani, W. A., Khan, M. M., Brabazon, D., Obeidi, M. A. and Ahad, I. U. 2023. The porosity design and deformation behavior analysis of additively manufactured bone scaffolds through finite element modelling and mechanical property investigations. *J. Funct. Biomater.*, **14**(10), 496.

Rezapourian, M. and Hussainova, I. 2023. Optimal mechanical properties of hydroxyapatite gradient Voronoi porous scaffolds for bone applications – a numerical study. *J. Mech. Behav. Biomed. Mater.*, **148**, 106232.

Rezapourian, M., Kamboj, N. and Hussainova, I. 2021. Numerical study on the effect of geometry on mechanical behavior of triply periodic minimal surfaces. *IOP Conf. Ser.: Mater. Sci. Eng.*, **1140**, 012038.

Rezapourian, M., Kamboj, N., Jasiuk, I. and Hussainova, I. 2022. Biomimetic design of implants for long bone critical-sized defects. *J. Mech. Behav. Biomed. Mater.*, **134**, 105370.

Rezapourian, M., Jasiuk, I., Saarna, M. and Hussainova, I. 2023. Selective laser melted Ti6Al4V split-P TPMS lattices for bone tissue engineering. *Int. J. Mech. Sci.*, **251**, 108353.

Rezapourian, M., Kumar, R. and Hussainova, I. 2024. Effect of unit cell rotation on mechanical performance of selective laser melted gyroid structures for bone tissue engineering. *Prog. Eng. Sci.*, **1**(2–3), 100011.

Su, S., Chen, W., Zheng, M., Lu, G., Tang, W., Huang, H. et al. 2022. Facile fabrication of 3D-printed porous Ti6Al4V scaffolds with a Sr-CaP coating for bone regeneration. *ACS Omega*, **7**(10), 8391–8402.

Verma, R., Kumar, J., Singh, N. K., Rai, S. K., Saxena, K. K. and Xu, J. 2022. Design and analysis of biomedical scaffolds using TPMS-based porous structures inspired from additive manufacturing. *Coatings*, **12**(6), 839.

Vigil, J., Lewis, K., Norris, N., Karakoç, A. and Becker, T. A. 2024. Design, fabrication, and characterization of 3D-printed multiphase scaffolds based on triply periodic minimal surfaces. *Adv. Polym. Technol.*, **2024**(1), 4616496.

Wang, C., Wu, J., Liu, L., Xu, D., Liu, Y., Li, S. et al. 2023. Improving osteoinduction and osteogenesis of Ti6Al4V alloy porous scaffold by regulating the pore structure. *Front. Chem.*, **11**, 1190630.

Wang, Z. and Li, P. 2018. Characterisation and constitutive model of tensile properties of selective laser melted Ti-6Al-4V struts for microlattice structures. *Mater. Sci. Eng. A*, **725**, 350–358.

Yang, X., Wu, L., Li, C., Li, S., Hou, W., Hao, Y. et al. 2024. Synergistic amelioration of osseointegration and osteoimmunomodulation with a microarc oxidation-treated three-dimensionally printed Ti-24Nb-4Zr-8Sn scaffold via surface activity and low elastic modulus. *ACS Appl. Mater. Interfaces*, **16**(3), 3171–3186.

Yin, C., Zhang, T., Wei, Q., Cai, H., Cheng, Y., Tian, Y. et al. 2021. Surface treatment of 3D printed porous Ti6Al4V implants by ultraviolet photofunctionalization for improved osseointegration. *Bioact. Mater.*, **7**, 26–38.

Zhang, C., Zhou, Z., Liu, N., Chen, J., Wu, J., Zhang, Y. et al. 2023. Osteogenic differentiation of 3D-printed porous tantalum with nano-topographic modification for repairing craniofacial bone defects. *Front. Bioeng. Biotechnol.*, **11**, 1258030.

Zhu, J., Zou, S., Mu, Y., Wang, J. and Jin, Y. 2022. Additively manufactured scaffolds with optimized thickness based on triply periodic minimal surface. *Materials*, **15**(20), 7084.

Luurakenduste mitmepinnaliste TPMS-võrede mehaaniline analüüs

Mansoureh Rezapourian ja Irina Hussainova

Minimaalse energiaga kolmikperioodiline pind (TPMS) võimaldab tänu oma kergesti kohandatavatele geomeetrilistele ja mehaanilistele omadustele kasutada seda luukoe asendusstruktuuride loomiseks. Uuringus viidi läbi viie kombineeritud pinnatüübiga ja minimaalse energiaga kolmikperioodilise pinnaga võreplaani – PDL, PNG, SDL, DNG ja PLG – mehaaniline analüüs. Kõnealused võreplaanid on kuue minimaalse energiaga kolmikperioodilise pinna (P – Primitiivne, D – Diamond, L – Lidinoid, G – Giroid, S – Split-P ja N – Neovius) kombinatsioonid, mis valmistati sulamist Ti6Al4V. Analüüsi eesmärk oli hinnata geomeetrilisi tunnuseid, nagu pindala (SA) ja pindala-mahu suhe (SA/VR), ning mehaanilisi omadusi, kaasa arvatud elastsusmoodul (E), voolepinge (Y), maksimaalne survetugevus (CM) ja energia neeldumine (EA), rakendades kvaasistaatilist survekatset. Tulemused näitasid, et kombineeritud pinnatüüpi võredel oli purunemine sujuvam, elastsusmoodul kõrgem ja geomeetrilised parameetrid tugevamad võrreldes üksikpinnatüüpi võredega. PLG-l oli kõrgeim EA väärtus, samal ajal kui SDL-il oli väga hea CM väärtus ning kõrgeimad SA ja SA/VR väärtused, mis näitab selle ülimat geomeetrilist keerukust. Üksikpinnatüüpi võredel, nagu D ja S, oli küll suurem E väärtus, aga need purunesid hapralt. Need tulemused demonstreerivad minimaalse energiaga kolmikperioodiliste pindade kombineerimise potentsiaali optimeeritud karkass-struktuuride konstrueerimiseks biomeditsiinitehnikas.